



Immune subtyping of extranodal NK/T-cell lymphoma: a new biomarker and an immune shift during disease progression

Junhun Cho¹ · Seok Jin Kim² · Woong-Yang Park³ · Jinho Kim³ · Jeongmin Woo^{3,4} · Gahyun Kim^{3,4} · Sang Eun Yoon² · Young Hyeon Ko¹ · Won Seog Kim²

Received: 28 July 2019 / Revised: 22 September 2019 / Accepted: 22 September 2019 / Published online: 25 October 2019
© The Author(s), under exclusive licence to United States & Canadian Academy of Pathology 2019

Abstract

Extranodal NK/T-cell lymphoma is an aggressive lymphoma that is strongly associated with Epstein–Barr virus infection. Although some extranodal NK/T-cell lymphoma patients have shown responses to immune checkpoint blockade, biomarkers for predicting extranodal NK/T-cell lymphoma patient response to immunotherapy have not yet been defined. To understand the tumor immune microenvironment, we analyzed the expression of 579 immune-related genes and characterized the immune cells using immunohistochemistries and in situ hybridization for EBER. Based on comprehensive analyses, we developed an immune subtyping model that classifies extranodal NK/T-cell lymphoma patients into four tumor immune microenvironment subgroups using three immunohistochemical markers (FoxP3, PD-L1, and CD68). The four tumor immune microenvironment subgroups were named immune tolerance, immune evasion-A, immune evasion-B, and immune silenced. The immune tolerance group was characterized by high-Treg counts and was frequently observed in early stage, and nasal extranodal NK/T-cell lymphoma. The immune evasion group showed high cytotoxic T-cell counts and high PD-L1 expression but low Treg counts. In the immune-silenced group, almost all immune responses were exhausted, most patients were at an advanced stage, and had the poorest disease prognosis among the tumor immune microenvironment subgroups. In some patients ($n = 3$), a shift in the tumor immune microenvironment subgroup classification was observed in sequential biopsies. The response rate to pembrolizumab, an anti-PD-1 antibody, was 100% (1/1) in the immune tolerance group, 60% (3/5) in the immune evasion group, and 0% (0/5) in the immune-silenced group. We classified extranodal NK/T-cell lymphoma into four tumor immune microenvironment subgroups using a new classification system. In conclusion, we propose that the tumor immune microenvironment of extranodal NK/T-cell lymphoma may change during disease progression and may serve as a useful biomarker for immunotherapy.

These authors contributed equally: Junhun Cho, Seok Jin Kim

These authors contributed equally: Young Hyeon Ko, Won Seog Kim

Supplementary information The online version of this article (<https://doi.org/10.1038/s41379-019-0392-8>) contains supplementary material, which is available to authorized users.

✉ Young Hyeon Ko
yhko310@skku.edu

✉ Won Seog Kim
wskimsmc@skku.edu

¹ Department of Pathology, Samsung Medical Center, Sungkyunkwan University School of Medicine, Seoul, Korea

Introduction

Since the early 2000s, new therapeutic approaches, such as nonanthracycline chemotherapy, concurrent chemoradiation therapy, and hematopoietic stem cell transplantation, have improved the outcomes of patients with extranodal NK/T-cell lymphoma. Despite these advances, extranodal NK/T-cell lymphoma remains one of the more clinically aggressive lymphomas [1]. A recent breakthrough in

² Division of Hematology and Oncology, Department of Medicine, Samsung Medical Center, Sungkyunkwan University School of Medicine, Seoul, Korea

³ Samsung Genome Institute, Samsung Medical Center, Sungkyunkwan University School of Medicine, Seoul, Korea

⁴ Samsung Advanced Institute for Health Sciences and Technology, Sungkyunkwan University School of Medicine, Seoul, Korea

immunotherapy has facilitated significant therapeutic achievements for several malignant tumors [2–6]. In extranodal NK/T-cell lymphoma, latent membrane proteins expressed by Epstein–Barr virus (EBV) infection can be targets for cytotoxic T-cells [7], suggesting that extranodal NK/T-cell lymphoma may be a good candidate for immunotherapy. Clinical trials for immune checkpoint blockade in extranodal NK/T-cell lymphoma are indeed underway, and some promising results have been reported [8–12]. To establish strategies for precision immunotherapy, understanding the tumor immune microenvironment is essential, but current knowledge about the tumor immune microenvironment in extranodal NK/T-cell lymphoma is not sufficient. The key questions that have not yet been solved regarding the tumor immune microenvironment of extranodal NK/T-cell lymphoma are presented below.

First, some papers have reported that PD-L1 is frequently expressed in extranodal NK/T-cell lymphoma tumors [8, 13–17] and that mutations in the *JAK/STAT* pathway, particularly in *STAT3*, are associated with PD-L1 upregulation in extranodal NK/T-cell lymphoma tumors [13]. However, there are many cases in which PD-L1 is expressed without a *STAT3* mutation. Moreover, the expression of PD-L1 in tumor-associated macrophages cannot be explained by oncogenic mutations in tumor cells.

Second, immune checkpoint blockade targeting the PD-1/PD-L1 axis is effective in some patients with extranodal NK/T-cell lymphoma [9, 10, 12]. However, biomarkers to screen for patients who will respond to this treatment have not been established. Indeed, although PD-L1 immunohistochemistry is being used as a screening tool in other solid tumors [18–20], the criteria for lymphomas, especially extranodal NK/T-cell lymphoma, are unclear. Moreover, there is a group of patients in whom the degree of PD-L1 expression and the therapeutic response are not well correlated [10–12].

In addition, one of the unresolved questions related to extranodal NK/T-cell lymphoma is why, unlike other aggressive lymphomas such as diffuse large B-cell lymphoma, extranodal NK/T-cell lymphoma is mostly found as a localized disease. Indeed, most aggressive lymphomas are usually found in advanced stages and have a high tumor burden. However, despite its aggressive behavior, extranodal NK/T-cell lymphoma is often confined to the upper aerodigestive tract at the time of first diagnosis.

In this study, we investigated the characteristics of the extranodal NK/T-cell lymphoma tumor immune microenvironment using a NanoString assay and immunohistochemistry in 95 extranodal NK/T-cell lymphoma patients. The patients were classified into tumor immune microenvironment subgroups by NanoString assay and we analyzed clinical characteristics and immunohistochemistry profile of each subgroup. After validating our results in 50

extranodal NK/T-cell lymphoma patients, we studied how the tumor immune microenvironment is related to the course of extranodal NK/T-cell lymphoma and investigated whether particular biomarkers can be used to select extranodal NK/T-cell lymphoma patients eligible for immunotherapy.

Materials and methods

Patient selection

Of the 283 patients diagnosed with extranodal NK/T-cell lymphoma in the Samsung medical center, Seoul, Korea between 2000 and 2014, 95 patients with available formalin-fixed paraffin-embedded tissue and medical records were studied in the training cohort (Fig. 1). Formalin-fixed paraffin-embedded tissues were used for NanoString assays, immunohistochemistry, and EBV in situ hybridization (ISH). Clinicopathological information, including age, sex, location, B symptoms, serum EBV DNA copy number, distal lymph node involvement, Ann Arbor stage, prognostic index of natural killer lymphoma (-EBV) [21], prior treatments, and survival data were evaluated by reviewing electronic medical records (Supplementary Table 1).

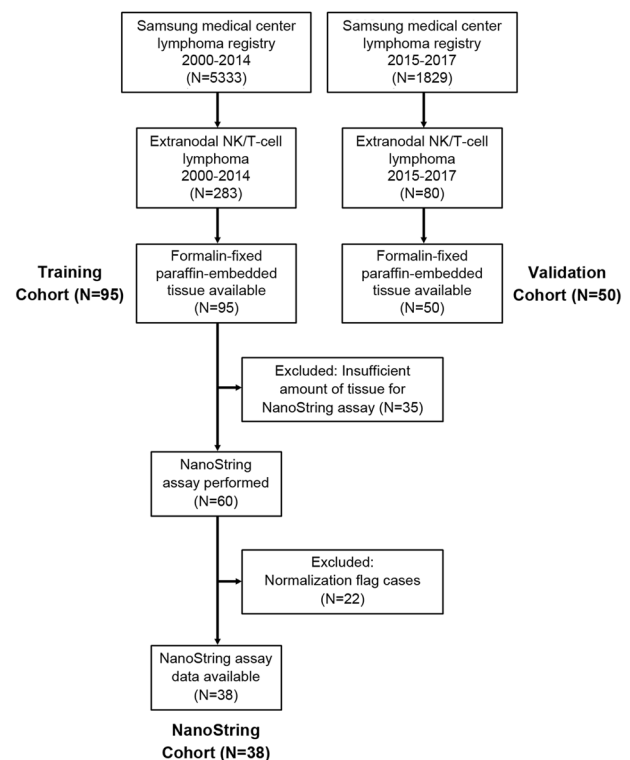


Fig. 1 The profile of the cohorts used in this study. There were 95 cases in the training cohort, 38 of which were NanoString cases, whose formalin-fixed paraffin-embedded tissue was successfully analyzed using a NanoString assay. The validation cohort included 50 cases

Of the 80 patients diagnosed with extranodal NK/T-cell lymphoma at the Samsung medical center between 2015 and 2017, 50 patients with available formalin-fixed paraffin-embedded tissue and medical records were studied in the validation cohort (Fig. 1). Clinicopathological features similar to those listed for the training cohort were evaluated (Supplementary Table 1). This study was approved by the institutional review board of Samsung medical center, Seoul, Korea.

NanoString nCounter assay

Of the 95 patients in the training cohort, RNA expression was analyzed using the nCounter® technology from NanoString in 60 cases with enough amount of specimens suitable for molecular studies. For the NanoString nCounter assay, we used the nCounter® Human Immunology V2 Panel with 579 human immune signature genes and 15 housekeeping genes (NanoString Technologies, Seattle, WA, USA). Total RNA was extracted from three to four- μ m-thick formalin-fixed paraffin-embedded tissue sections from representative blocks using the High Pure RNA Paraffin kit (Roche Diagnostic, Mannheim, Germany). RNAs (200 ng) were hybridized to target sequence-specific capture probes and fluorescence-labeled reporter probes. The mRNA-probe complexes were washed, immobilized, and quantified by fluorescence imaging. To remove the batch effect of nCounter gene expression, we performed two-step normalizations for the gene expression matrix. First, within-normalization using the NanoStringNorm R package with options CodeCount + Sum, Background = mean, and SampleContent = total.sum was performed, and outliers were adjusted to the median value with the outlier R package [22]. Next, gene expression matrixes spanning two batches were rescaled by between-normalization using the edgeR R package, and \log_{10} transformed expression was considered as the final gene expression matrix [23]. One hundred and four genes with very low mean expression (<1, less than the normalized data 10) were removed from the analysis, a heatmap was made for 475 genes, and hierarchical clustering was performed (<https://software.broadinstitute.org/morpheus/>).

Immunohistochemistry and in situ hybridization

EBV ISH followed by immunohistochemistry for PD-L1 (clone SP142; Ventana, Tucson, AZ, USA) was performed to identify the types of cells expressing PD-L1. Detailed information about the PD-L1 and EBER (INFORM EBER Probe, Ventana, AZ, USA) stains is presented in Supplementary Table 2. After PD-L1 staining, the percentage of tumor cells expressing PD-L1 was measured. Although it was not possible to accurately count the number of tumor-

associated macrophage expressing PD-L1, the number of tumor cells and the number of PD-L1-positive tumor-associated macrophage in the region where tumor cells were present were roughly evaluated, and the ratio of the approximate number of total PD-L1-positive tumor-associated macrophage /number of EBER-positive tumor cells $\times 100$ was calculated. For example, when the number of PD-L1-positive tumor-associated macrophage was considered to be similar to that of tumor cells in the area, the ratio was evaluated as 100. When PD-L1-positive tumor-associated macrophage appeared to comprise 1/10 of the tumor cells, the ratio was 10. When the number of PD-L1-positive tumor-associated macrophage was approximately twice the number of tumor cells, the ratio was 200. Finally, the PD-L1 expression values of tumor cells and tumor-associated macrophage were summed and used as the PD-L1 score.

To investigate the composition of immune cells that surround extranodal NK/T-cell lymphoma tumors, immunohistochemistry was performed on tissue from the training cohort using stains for CD68 (clone 514H12, Leica Biosystems, IL, USA) and CD163 (clone 10D6, Thermo Fisher Scientific, CA, USA) (for macrophages), CD8 (clone SP57, Ventana, AZ, USA) (for cytotoxic T-cells) and FoxP3 (clone 236 A/E7, Abcam, Cambridge, UK) (for Treg). Details of the immunohistochemistry stains are given in Supplementary Table 3. The number of positive cells was counted manually after photographing one representative field with the highest tumor cell density per immunohistochemistry slide, visualized at $\times 40$ magnification. The area of the image was $60,000 \mu\text{m}^2$ ($300 \times 200 \mu\text{m}$). In practice, the field is viewed directly under a microscope without collecting an image, so the area was multiplied by 3.33 to reach a value of $\sim 200,000 \mu\text{m}^2$ (0.2 mm^2), the area of a field under a microscope at a $\times 40$ magnification.

In the validation cohort, CD68, FoxP3, and PD-L1 immunostaining were performed in the same manner described for the training cohort. PD-L1 staining was conducted using a single staining procedure without EBER, and the EBER slides were evaluated together with the tumor area and tumor cell density to calculate the PD-L1 score following the same procedure as described for the training cohort.

Statistical analyses

We used the SPSS 24.0 statistical software program (IBM Corporation) for statistical analyses. Pearson's chi-square test or linear-by-linear association was used for crossover analysis of clinicopathological features. A Kaplan–Meier curve (log-rank test) was used for survival analysis. Pearson's correlation test was used to analyze the correlation between two continuous variables. When comparing two or

more groups of continuous variables, the Mann–Whitney test for two groups or the Kruskal–Wallis test for more than two groups was performed. *P* values <0.05 were considered statistically significant.

Results

NanoString assay and hierarchical clustering

Using the heatmap from the NanoString assay, 38 patients were divided into four clusters (A, B1, B2, and C) (Fig. 2a). There were no significant differences in age, sex, or location among the clusters. However, statistically significant differences were found in serum EBV DNA copy number (*P* = 0.014), Ann Arbor stage (*P* = 0.035), and prognostic index of natural killer lymphoma [21] (*P* = 0.023). Cluster A was associated with the absence of serum EBV DNA detection, early stage, and the low-risk group. Cluster C showed the opposite pattern of cluster A. Table 1 summarizes the clinicopathological features of the four NanoString clusters.

We next evaluated the activity of major immune-related genes across each NanoString cluster (Fig. 2b). In cluster A, *CCL22* expression was high, and the expression of *FOXP3* and *ICOS* were also high. *CD274*, *IDO1* and *CD276*, which are representative inhibitory immune checkpoint genes, showed the highest activity in cluster B1 relative to the other clusters. Among the *KIR* family of immune checkpoint genes, *KIR*-activating subgroup 1 genes (including *KIR3DS1*, *KIR2DS1*, *KIR2DS2*, and *KIR2DS4*) were most highly expressed in cluster B1, whereas *KIR*-inhibiting subgroup 2 genes (including *KIR2DL3*, *KIR2DL4*, *KIR2DL5*, *KIR3DL3*, *KIR2DL1*, *KIR2DL2*, *KIR3DL1*, and *KIR3DL2*) were most highly expressed in cluster B2. Moreover, *KLRG1* had the lowest expression in cluster B2. The expression of *IFNG* and *GZMB*, which are surrogate markers of immune activity, was highest in cluster B2. In cluster C, the expression of most genes was decreased, but *KLRG1* and *MIF* showed high expression in cluster C.

Double procedure for PD-L1 (SP142) immunohistochemistry and EBV in situ hybridization

Of the 95 cases, more than 50% and 10% tumor cell positivity for PD-L1 was observed in two cases (2%) and six cases (6%), respectively, and 61 cases (64%) were completely negative for PD-L1 in tumor cells. Concerning the PD-L1 score for tumor-associated macrophage (PD-L1 tumor-associated macrophage score), 24 cases (25%) had scores above 100, 57 cases (60%) had scores above 10, and 19 cases were completely negative (20%). The mean PD-L1

score (tumor cell PD-L1 expression plus PD-L1 tumor-associated macrophage score) in the training cohort was 65.8, and the median value was 30.0. The PD-L1 score was above 100 in 29 cases (31%) and above 10 in 59 cases (62%). These values were lower than the PD-L1-positive rates (varies according to cutoff value) reported in previously published papers on extranodal NK/T-cell lymphoma [8, 14–17]. Thus, we compared the quality of PD-L1 staining in PD-L1/EBER double-stained slides with that in PD-L1 single-stained slides in all patients to identify potential false-negative artifacts due to staining combined with EBV ISH. We found no significant difference in PD-L1 expression levels assessed via analysis of double-versus single-stained slides. (Supplementary Fig. 1).

Quantitative assessment of immune cells by immunohistochemistry

The mean cell counts (per high-power field (/HPF)) of CD68, CD163, CD8, and FoxP3-positive cells were 580, 667, 891, and 153, respectively. The numbers of CD68, CD163, and CD8 positive cells was slightly higher in cluster B1 than A, and lower in cluster C than A. Moreover, FoxP3 expression was the highest in cluster A and decreased toward cluster C (Fig. 2c). The CD68-positive cell counts and CD163 positive cell counts were positively correlated ($R^2 = 0.682$, $P < 0.001$, graph not shown). In cluster C, inflammatory cells, including CD8 + cytotoxic T-cell, were relatively rare. In four of five cluster C cases, process-type macrophages were predominant (>90%) in CD68 staining. Process-type macrophage refers to the macrophage consisting of a small cell body and dendritic processes with a small amount of cytoplasm, resulting in fusiform shape. The morphology of these macrophages in the CD68 staining was similar to that in the CD163 staining.

Development of a classification system using immunohistochemistry

Based on the above results, we developed a classification system to classify tumor immune microenvironment subgroups using immunohistochemistry, and we applied this classification system to the training cohort (Fig. 3a). The typical immunohistochemistry pattern of each subgroup is depicted in Fig. 3b. The groups corresponding to NanoString clusters A, B1, B2, and C that came out of this classification system were named immune tolerance (IT), immune evasion A (IE-A), immune evasion B (IE-B), and immune silenced (IS), respectively. When the training cohort was classified into subgroups using the classification system, the IT, IE-A, IE-B, and IS groups included 13 cases (14%), 49 cases (52%), 25 cases (26%), and 8 cases (8%),

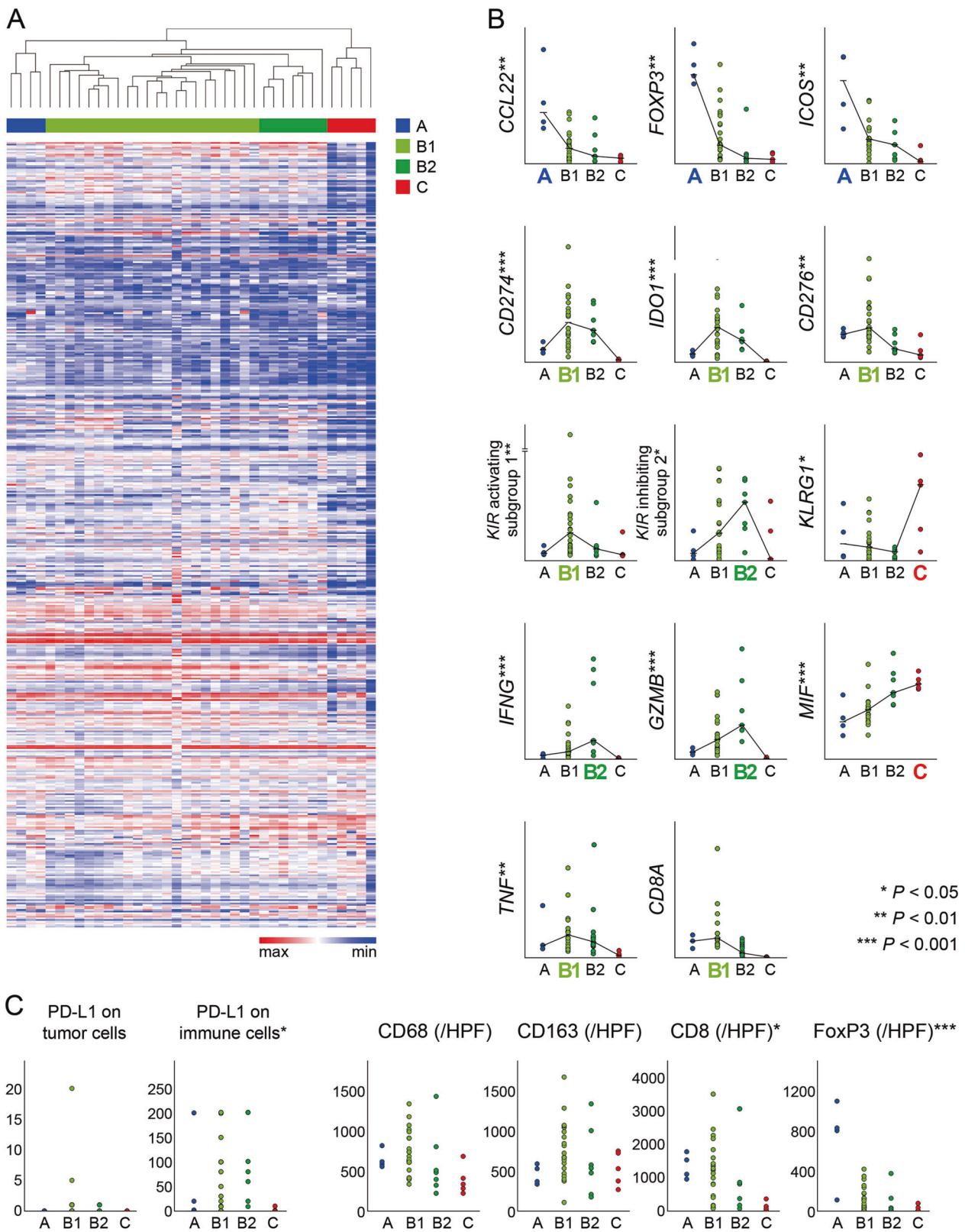


Fig. 2 **a** Heatmap and hierarchical clustering of the NanoString cohort based on NanoString assay results. NanoString clusters A, B1, B2, and C included 4, 22, 7, and 5 cases, respectively. **b** Comparison of the expression levels of key genes of interest across clusters. The line

graph represents the median value for each cluster. **c** Number of inflammatory cells per high-power field in each cluster determined by immunohistochemistry. HPF high-power field

Table 1 Clinicopathological characteristics of the patients in each cohort divided into immunologic clusters (NanoString clusters or tumor immune microenvironment subgroups)

	NanoString cohort (N = 38)					Training cohort (N = 95)					Validation cohort (N = 50)					
	NanoString clusters (%)					tumor immune microenvironment subgroups (%)					tumor immune microenvironment subgroups (%)					
	A (N = 4)	B1 (N = 22)	B2 (N = 7)	C (N = 5)	Total	IT (N = 13)	IE-A (N = 49)	IE-B (N = 25)	IS (N = 8)	Total	IT (N = 6)	IE-A (N = 32)	IE-B (N = 8)	IS (N = 4)	Total	P
Sex					0.943					0.979						
Male	3 (10.0)	18 (60.0)	5 (16.7)	4 (13.3)	30	9 (13.8)	33 (50.8)	17 (26.2)	6 (9.2)	65	5 (14.3)	23 (65.7)	5 (14.3)	2 (5.7)	35	0.674
Female	1 (12.5)	4 (50.0)	2 (25.0)	1 (12.5)	8	4 (13.3)	16 (53.3)	8 (26.7)	2 (6.7)	30	1 (6.7)	9 (60.0)	3 (20.0)	2 (13.3)	15	0.283
Age										0.748						
<60	4 (12.9)	19 (61.3)	4 (12.9)	4 (12.9)	31	10 (14.9)	36 (53.7)	16 (23.9)	5 (7.5)	67	5 (14.7)	19 (55.9)	6 (17.6)	4 (11.8)	34	
≥60	0 (0.0)	3 (42.9)	3 (42.9)	1 (14.3)	7	3 (23.1)	13 (46.4)	9 (32.1)	3 (10.7)	28	1 (6.3)	13 (81.3)	2 (12.5)	0 (0.0)	16	0.005
Location					0.276					0.289						
Nasal	2 (9.1)	14 (63.6)	5 (22.7)	1 (4.5)	22	11 (18.0)	29 (47.5)	17 (27.9)	4 (11.8)	61	5 (13.5)	25 (67.6)	7 (18.9)	0 (0.0)	37	
Others	2 (12.5)	8 (50.0)	2 (12.5)	4 (25.0)	16	2 (5.9)	20 (58.8)	8 (23.5)	4 (11.8)	34	1 (7.7)	7 (3.8)	1 (7.7)	4 (30.8)	13	0.110
LDH					0.486					0.473						
Elevated	1 (6.7)	7 (46.7)	4 (26.7)	3 (20.0)	15	4 (8.7)	23 (50.0)	14 (30.4)	5 (10.9)	46	1 (3.4)	22 (75.9)	4 (13.8)	2 (6.9)	29	
Not elevated	3 (13.6)	14 (63.6)	3 (13.6)	2 (9.1)	22	8 (17.8)	24 (53.3)	10 (22.2)	3 (6.7)	45	5 (23.8)	10 (47.6)	4 (9.0)	2 (9.5)	21	0.589
B symptoms					0.268					0.933						
Present	2 (22.2)	3 (33.3)	3 (33.3)	1 (11.1)	9	3 (15.0)	11 (55.0)	5 (25.0)	1 (5.0)	20	0 (0.0)	8 (72.7)	2 (18.2)	1 (9.1)	11	
Absent	2 (7.1)	18 (64.3)	4 (14.3)	4 (14.3)	28	10 (13.5)	38 (51.4)	19 (25.7)	7 (9.5)	74	6 (15.4)	24 (61.5)	6 (15.4)	3 (7.7)	39	0.204
Serum EBV					0.014					0.003						
Detected	0 (0.0)	6 (46.2)	2 (15.4)	5 (38.5)	13	2 (5.4)	15 (40.5)	13 (35.1)	7 (18.9)	37	3 (7.7)	25 (64.1)	7 (17.9)	4 (10.3)	39	
Not detected	3 (14.3)	13 (61.9)	5 (23.8)	0 (0.0)	21	11 (22.9)	27 (56.2)	9 (18.8)	1 (2.1)	48	3 (30.0)	6 (60.0)	1 (10.0)	0 (0.0)	10	0.054
Distal lymph node					0.075					0.003						
Involved	1 (14.3)	2 (28.6)	1 (14.3)	3 (42.9)	7	0 (0.0)	5 (29.4)	8 (47.1)	4 (23.5)	17	6 (18.2)	23 (69.7)	2 (6.1)	2 (6.1)	33	
Not involved	3 (10.0)	19 (63.3)	6 (20.0)	2 (6.7)	30	13 (17.1)	43 (56.6)	16 (21.1)	4 (5.3)	76	0 (0.0)	5 (50.0)	3 (30.0)	2 (20.0)	10	0.005
Ann Arbor stage					0.035					0.014						
I-II	3 (13.6)	14 (63.6)	5 (22.7)	0 (0.0)	22	12 (21.8)	29 (52.7)	12 (21.8)	2 (3.6)	55	6 (19.4)	22 (71.0)	3 (9.7)	0 (0.0)	31	
III-IV	1 (6.7)	7 (46.7)	2 (13.3)	5 (33.3)	15	1 (2.6)	19 (50.0)	12 (31.6)	6 (15.8)	38	0 (0.0)	10 (52.6)	5 (26.3)	4 (21.1)	19	0.010 ^a
prognostic Index of Natural Killer Cell Lymphoma					0.023 ^a					0.003 ^a						
Low	3 (17.6)	10 (58.8)	4 (23.5)	0 (0.0)	17	9 (23.1)	20 (51.3)	9 (23.1)	1 (2.6)	39	5 (25.0)	12 (60.0)	3 (15.0)	0 (0.0)	20	
Intermediate	0 (0.0)	9 (81.8)	1 (9.1)	1 (9.1)	11	3 (13.0)	14 (60.9)	4 (17.4)	2 (8.7)	23	0 (0.0)	8 (80.0)	2 (20.0)	0 (0.0)	10	
High	1 (11.1)	2 (22.2)	2 (22.2)	4 (44.4)	9	1 (3.1)	15 (46.9)	11 (34.4)	5 (15.6)	32	1 (5.0)	12 (60.0)	3 (15.0)	4 (20.0)	20	

IT immune tolerance, *IE* immune evasion, *IS* immune silenced, *LDH* lactate dehydrogenase, *EBV* Epstein-Barr virus

^aLinear-by-linear association

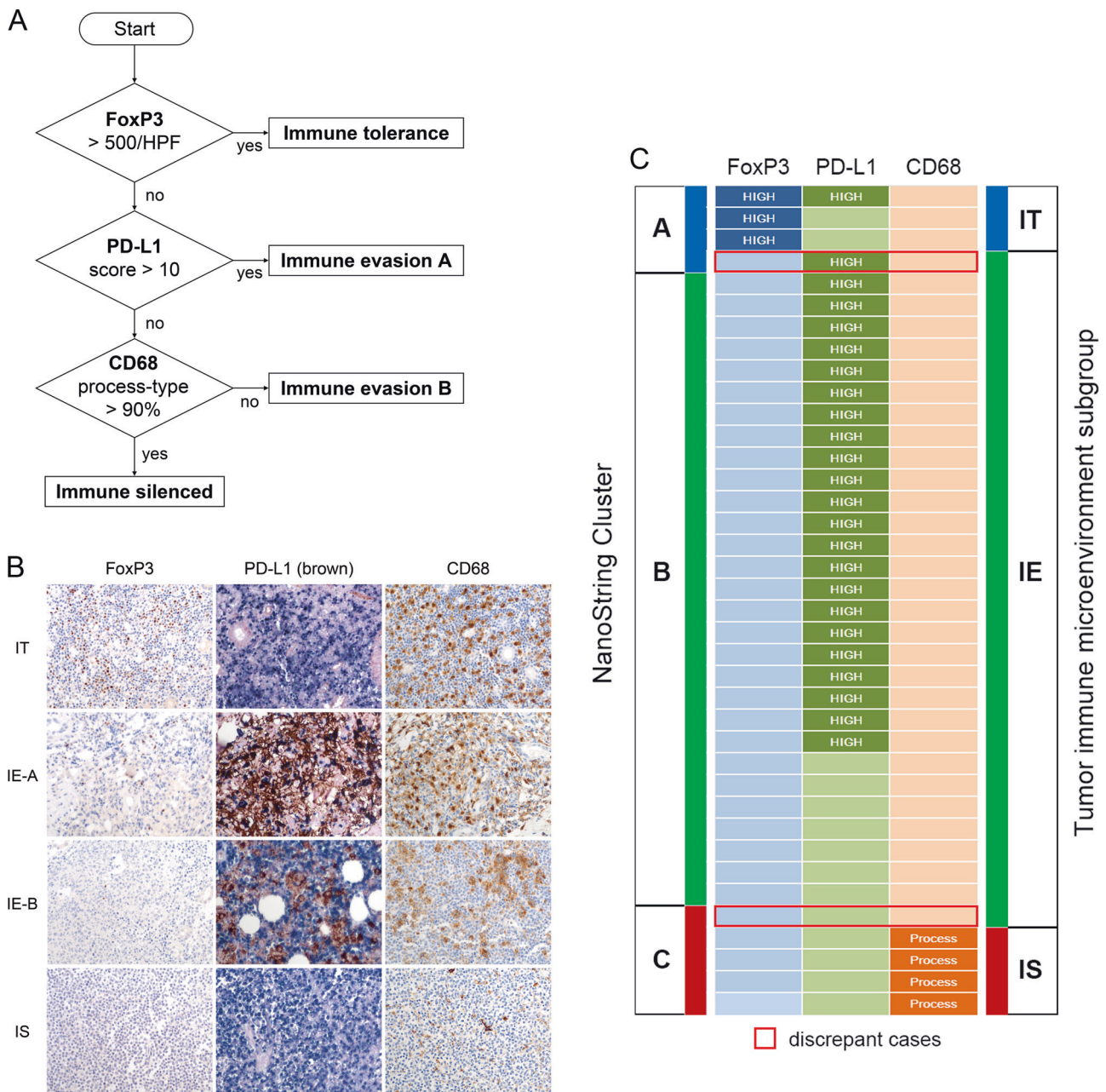


Fig. 3 **a** Based on the results of the NanoString assay, we defined four novel extranodal NK/T-cell lymphoma tumor immune microenvironment subgroups using three types of immunohistochemical staining (FoxP3, PD-L1, and CD68). The subgroups identified according to this protocol were named immune tolerance, immune evasion A, immune evasion B, and immune silenced, according to their immunologic features. **b** Representative immunohistochemistry images of each tumor immune microenvironment subgroup. FoxP3-positive regulatory T-cells are very abundant in IT but then decrease rapidly.

PD-L1 expression is highest in IE-A patients. The CD68-positive macrophages of IS show a unique morphology of the process type. **c** Comparison of NanoString clusters (A, B, and C) and the tumor immune microenvironment subgroups (IT, IE, and IS) generated by our classification system. Thirty six of thirty eight cases (94%) were matched and there were two (6%) discordant cases. HPF high-power field, IT immune tolerance, IE-A immune evasion A, IE-B immune evasion B, IS immune silenced

respectively. When comparing NanoString clusters (A, B, and C) and the tumor immune microenvironment subgroups (IT, IE, and IS) generated by our classification system, 36 of 38 cases (94%) were matched. (Fig. 3c) Histologically, extensive necrosis was identified in 3 cases (23%), 27 cases

(55%), 8 cases (32%), and 0 case (0%) in IT, IE-A, IE-B, and IS groups, respectively. In all eight cases of IS group, even focal necrosis was not identified. (Supplementary Table 4) In the IT subgroup, stage I–II cases accounted for 92% of samples and prognostic index of natural killer

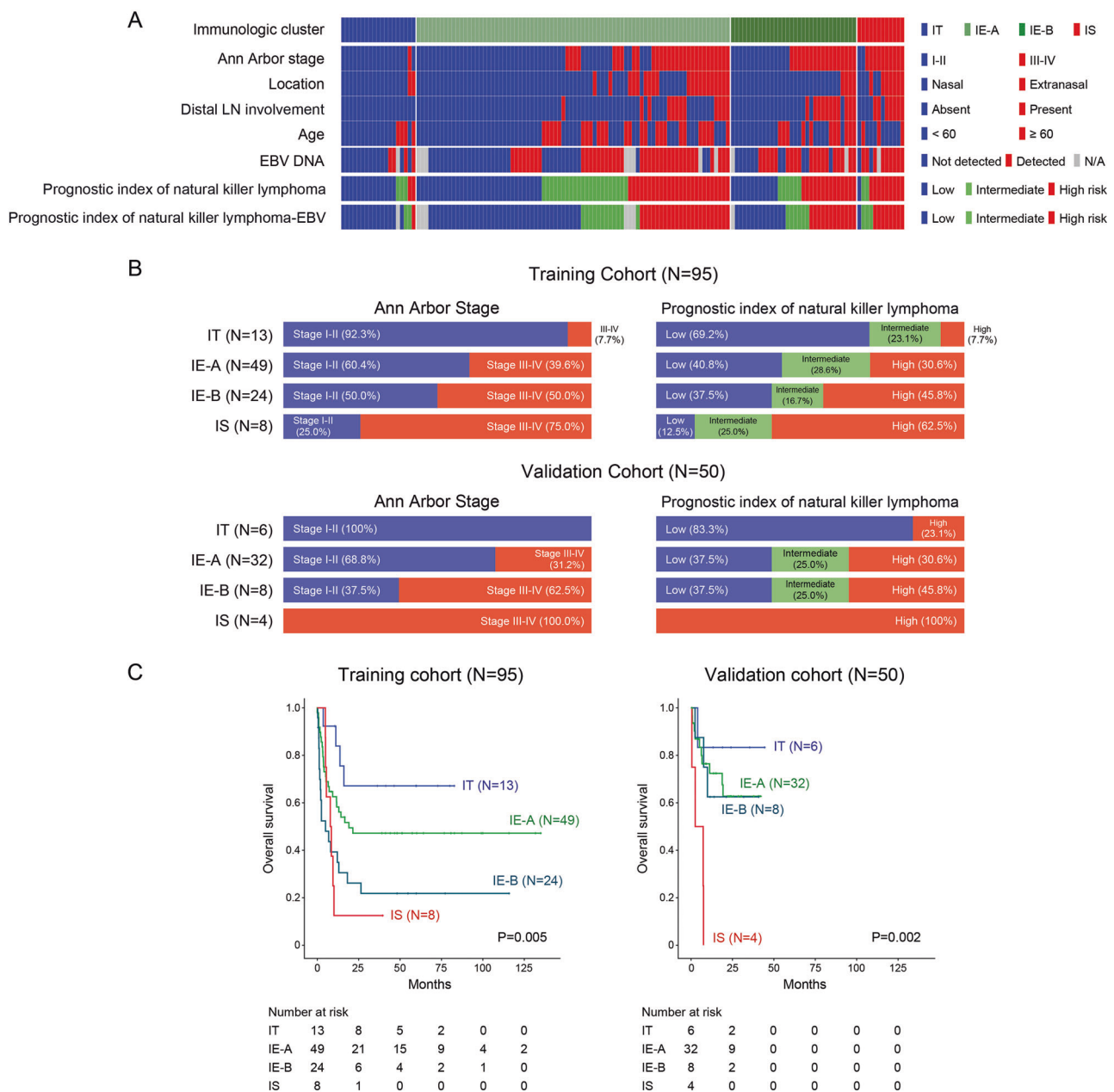


Fig. 4 a Clinical heatmap for all patients (training and validation cohorts). **b** Bar graphs comparing the Ann Arbor stage and prognostic index of natural killer lymphoma risk classification across tumor immune microenvironment subgroups in the training cohort and validation cohort. **c** Kaplan–Meier curves of overall survival for each

tumor immune microenvironment subgroup in the training cohort and validation cohort. The IT group showed the best prognosis and the IS group the worst in both training and validation cohorts. IT immune tolerance, IE immune evasion, IS immune silenced, LN lymph node, EBV Epstein–Barr virus

lymphoma low-risk cases accounted for 69% of samples. In contrast, 75% and 63% of IS patients were stage III–IV and prognostic index of natural killer lymphoma high-risk, respectively. Both the Ann Arbor stage and prognostic index of natural killer lymphoma showed consistent trends in the order IT, IE-A, IE-B, and IS (Fig. 4a). Survival was also highest in the IT subgroup and lowest in IS patients (Fig. 4b, c). To verify the accuracy of this immunohistochemistry-based classification system, we next

applied it to the validation cohort ($N = 50$). The training and validation cohort were diagnosed at different times, but there was no statistically significant difference in clinicopathological characteristics. (Supplementary Table 1) In the validation cohort, the IT, IE-A, IE-B, and IS subgroups contained 6 (12%), 32 (64%), 8 (16%), and 4 (8%) patients, respectively, proportions very similar to those observed in the training cohort. The Ann Arbor stage, prognostic index of natural killer lymphoma, and prognostic data for each

subgroup from the validation cohort were also consistent with those from the training cohort.

The examination of sequential biopsies and immune shift

Formalin-fixed paraffin-embedded blocks from sequential biopsy specimens were available for three patients from the training cohort. immunohistochemistry conducted on specimens collected at different time points (1.8–11.5 months apart) showed differences in the expression of FoxP3 and PD-L1 over time (Fig. 5a). Case #1 was classified as IT

based on analysis of the first biopsy due to its high number of FoxP3-positive cells. Immunohistochemistry conducted on the biopsy obtained 11.5 months later, however, showed no FoxP3-positive cells, and thus the second biopsy corresponded to IE-A according to our classification system. In Case #2, FoxP3-positive cells decreased from 1080/HPF in the first biopsy to 178/HPF in the second biopsy obtained 2.9 months later. There was an immune shift from IT to IE-A. Finally, in Case #3, while there was no shift in subgroup classification, PD-L1, which was not expressed in tumor cells in the initial biopsy, began to be expressed abruptly in the subsequent biopsy (PD-L1 score 100→180).

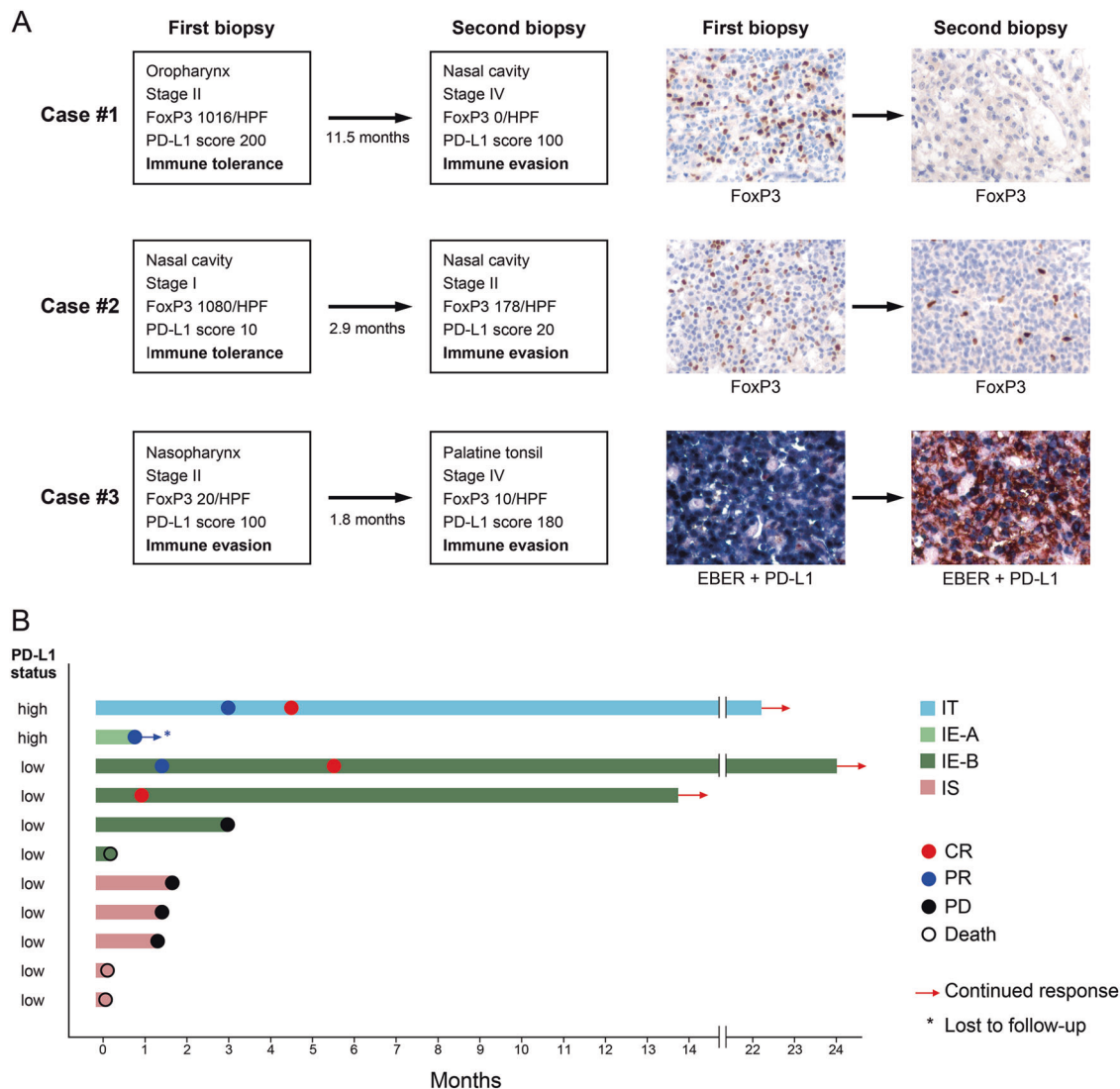


Fig. 5 a Immunohistochemistry staining results for three patients from whom serial biopsies were obtained. In Case #1 and #2, the expression of FoxP3 was reduced in tissue from the first biopsy versus the second, and in case #3, PD-L1 expression in EBER-positive tumor cells was observed in the second biopsy, but not the first. **b** Swimmer's plot showing the response of 11 extranodal NK/T-cell lymphoma patients

receiving pembrolizumab. In the IT, IE-A, and IE-B groups, some patients showed responses to pembrolizumab, but among the IS group, no patients showed a response. HPF high-power field, EBER Epstein–Barr virus-encoded small RNA, IT immune tolerance, IE-A immune evasion A, IE-B immune evasion B, IS immune silenced, CR complete response, PR partial response, PD progressive disease

Response to pembrolizumab according to tumor immune microenvironment subgroup

We next investigated how 11 refractory or recurrent extranodal NK/T-cell lymphoma patients responded to the anti-PD-1 agent pembrolizumab (dose of 100 mg, treatment cycle was repeated every 3 weeks) in a validation cohort. (Supplementary Table 5) The tumor immune microenvironment subgroup of each patient was determined, and their response to pembrolizumab was assessed using 2-deoxy-2-fluorine-18-fluoro-D-glucose positron emission tomography integrated with computed tomography according to standard criteria. One IT patient achieved complete remission (CR) and maintained this response for more than 15 months. Three of five IE patients showed a response, and indeed the two IE-B patients who achieved CR had durable responses of more than 12 and 19 months. All five IS patients showed no response to pembrolizumab (Fig. 5b).

Discussion

In this study, we classified extranodal NK/T-cell lymphoma patients into four subgroups according to the results obtained from a NanoString assay of a panel of 579 immune-related genes. Based on the immunopathologic characteristics of each group, we developed a new classification system that divides extranodal NK/T-cell lymphoma patients into four tumor immune microenvironment subgroups using three immunohistochemistry markers (FoxP3, PD-L1, and CD68).

The most representative pathologic feature of NanoString cluster A is a high-Treg count and *FOXP3* expression. High-Treg counts suppress peritumoral cytotoxic T-cells activity, so we named this subgroup “immune tolerance” or “IT”. IT patients were clinically characterized as having early Ann Arbor stage disease, nasal extranodal NK/T-cell lymphoma, and the best prognosis. Although the reason for elevated Treg counts in IT patients is unclear, several studies have shown that EBV infection is associated with high-Treg infiltration in both benign and malignant conditions [24–27]. *CCL22*, which has been shown to recruit Tregs in EBV-infected cells [28], also showed higher levels of expression in cluster A than in other clusters. In other words, high Treg can be considered as the strategies by which EBV-infected T/NK cells escaping host immunity are maintained in this group of patients, which supports the hypothesis that IT represents early-stage extranodal NK/T-cell lymphoma. These results are somewhat unexpected, as theoretically Tregs promote tumor progression by inhibiting antitumor immunity. In 2009, Kim et al. reported that high-Treg counts are a good independent prognostic marker of extranodal NK/T-cell lymphoma [29]. In this study, high-

Treg extranodal NK/T-cell lymphoma was associated with nasal location (statistically significant) and early stage (not statistically significant). In our opinion, the prognosis of high-Treg extranodal NK/T-cell lymphoma is better because most of the tumors in this group are early extranodal NK/T-cell lymphoma.

NanoString cluster B showed intermediate clinicopathological features between those of clusters A and C. The most prominent characteristic of cluster B is the high expression of inhibitory immune checkpoint markers, such as *CD274*, accompanied by active immune reactions. Thus, we named this tumor immune microenvironment subgroup “immune evasion” or “IE”.

The IE subgroup showed the highest expression of PD-L1. There are two known mechanisms of PD-L1 expression: intrinsic (induced by oncogenic mutation) and extrinsic (induced by external stimuli) pathways [30]. In a previous study, it was suggested that extranodal NK/T-cell lymphoma expresses PD-L1 through mutation of the *JAK/STAT* signaling pathway during tumorigenesis [13]. However, PD-L1 expression may also be upregulated by external stimuli such as interferon gamma [31, 32]. Indeed, interferon gamma induces PD-L1 expression on macrophages [32, 33]. In our study, all patients that showed PD-L1 positivity in tumor cells also showed PD-L1 positivity in tumor-associated macrophage, suggesting the presence of common external stimuli. In addition, in the serial biopsy case #3, tumor cells that were negative for PD-L1 in the initial biopsy expressed PD-L1 in the subsequent biopsy, suggesting PD-L1 expression on tumor cells may change with disease progression.

We divided NanoString cluster B into two subgroups, B1 and B2. The number of cytotoxic T-cells and the expression of immune checkpoint genes such as *CD274*, *IDO1*, and *CD276* were lower in cluster B2 compared with B1. PD-L1 tumor cell positive patients, although few, were mostly concentrated in cluster B1. Thus, in our model, PD-L1 expression by immunohistochemistry was used as a criterion for dividing clusters B1 and B2. Clusters B1 and B2 correspond to tumor immune microenvironment subgroups IE-A and IE-B, respectively.

NanoString cluster C showed decreases in most immune cells and no necrosis. After immunostaining of this group, few inflammatory cells other than process-type macrophages were observed, indicating the depletion of the immune response. Therefore, this group was named “immune silenced” or “IS”. IS was associated with an advanced disease stage, the high-risk group in prognostic index of natural killer lymphoma, and a very poor prognosis, suggesting that IS represents late extranodal NK/T-cell lymphoma. Also, the absence of necrosis in this group suggests that tissue necrosis, one of the characteristics of extranodal NK/T-cell lymphoma, may be attributed to anti-

tumoral host immunity. Results from the NanoString assay of cluster C showed that almost all immune-related gene expression was markedly decreased in these patients, except for a few genes, such as *MIF*. The mechanism of IS formation is not yet clear, but we hypothesize that it may involve T-cell exhaustion [34] or the selective survival of tumor cells. The original concept of immunoediting is that the cancer undergoes an elimination phase during the early stage of tumorigenesis, goes through the equilibrium phase and enters into the escape phase [35]. This phenomenon may occur similarly during progression of the tumor [36, 37]. Alternatively, perhaps an unidentified factor actively suppresses the immune response in IS. For example, MIF (macrophage migration inhibitory factor) has various biological activities [38], and one of these activities is to recruit myeloid-derived suppressor cells (MDSC), which cause immune suppression [39]. In malignant melanoma [40], MIF suppresses T-cell activation through circulating MDSC. 4-IPP (4-iodo-6-phenylpyrimidine), a small molecule MIF antagonist, has been shown to reduce MDSC-mediated suppression of T-cell activation and interferon gamma production in advanced-stage melanoma [41]. MIF antagonists might be considered a potential treatment option for extranodal NK/T-cell lymphoma patients with IS, which do not respond to immune checkpoint blockade.

Our results may suggest that IT, IE-A, IE-B, and IS represent sequential stages of extranodal NK/T-cell lymphoma disease progression. First, the Ann Arbor stages and prognostic index of natural killer lymphoma(-EBV) risk groups worsen from IT to IS subgroups. The second reason is the causal explanation. The hypothesis is as follows. EBV-infected T/NK cells in the nasal cavity are exposed to host immune surveillance and secrete chemokines (e.g., CCL22) to recruit Tregs for immune evasion. Surviving EBV-infected T/NK cells begin proliferating uncontrollably after a tumorigenic driver mutation has occurred. As Tregs decrease in number, tumor cell mutations accumulate, immunogenic neoantigens increase, and cytotoxic T-cells attack the tumor cells. As a countermeasure against this attack, tumor cells and surrounding tumor-associated macrophages express PD-L1. Upon reaching the IS stage during the immune suppressive process, the tumor cells proliferate rapidly and disseminate systemically in the absence of immune surveillance. These hypothetical steps are schematically illustrated in Fig. 6. The third reason is the changes in tumor immune microenvironment subgroups that were observed in serial biopsies. A shift in classification from IT to IE was observed in two patients. While the third patient remained IE over time, an increase in PD-L1 expression was noted between the first and second biopsy.

PD-L1 is an important biomarker that is widely used for patient selection for anti-PD-1/PD-L1 blockade via

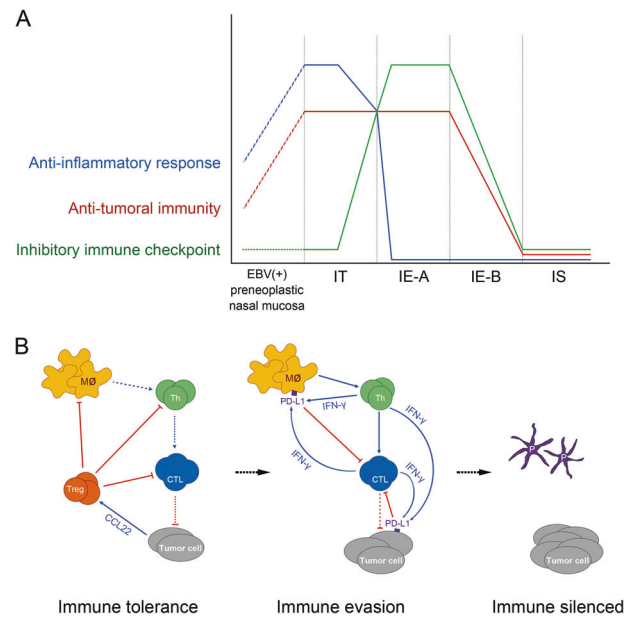


Fig. 6 **a** Schematic depicting the hypothesized mechanisms underlying extranodal NK/T-cell lymphoma progression. In the EBV-positive preneoplastic nasal mucosa, EBV-infected cells recruit Tregs. In IT, inflammatory cell infiltration is high, but their activity is inhibited by Tregs. When the number of Tregs decrease, the activity of cytotoxic T-cells increases, and PD-L1 expression rises (IE-A). Patients then progress to IE-B, in which the inflammatory response is gradually declining, and eventually to IS, in which almost all immune functions are suppressed. **b** Schematic illustrations of the immune response occurring in each tumor immune microenvironment subgroup. In IT, Tregs recruited by tumor cells suppress other immune responses. In IE, cytotoxic T-cells are active, but PD-L1 expression in tumor cells and tumor-associated macrophages is induced, suppressing cytotoxic T-cells activity and proliferation. In IS, almost all immune cells are absent, and only process-type macrophages remain. The function and role of these cells is not yet known. The blue line indicates positive effects, and the red line indicates negative effects. The dotted line indicates that the effect is weak. EBV Epstein-Barr virus, IT immune tolerance, IE immune evasion, IS immune silenced, MΦ macrophage, Th helper T-cell, CTL cytotoxic T-cell, Treg regulatory T-cell, P process-type macrophage

immunotherapy. However, in our data, two of three patients in the IE-B group, which is a low PD-L1 expression group, showed a durable complete response to pembrolizumab. While these are low-sample sizes, the results suggest that PD-L1 alone may not be sufficient for the detection of extranodal NK/T-cell lymphoma patients who will respond to immunotherapy.

CD68 is the most useful marker for identifying the IS group, and it is the only marker that can select a patient group that will not respond to an anti-PD-1 agent. The dominant distribution of process-type macrophages is a unique finding that is not often observed in general CD68 staining, except for microglia in central nervous system. CD68 staining of process-type macrophages are presented in Supplementary Fig. 2.

In this study, we first suggested the possibility of an immune shift during disease progression in extranodal NK/T-cell lymphoma. This is a new perspective on the tumor immune microenvironment that has not been described previously. In addition, our new classification system for defining tumor immune microenvironment subgroups is expected to be a useful tool for the selection of extranodal NK/T-cell lymphoma patients who will respond to immunotherapy. Moreover, further studies are required to investigate whether our tumor immune microenvironment model is applicable to other lymphomas and nonhematopoietic malignant tumors.

Acknowledgements This work was supported by grants from the National Research Foundation of Korea (NRF) funded by the Korea government (Ministry of Science and ICT) (grant number: 2017RIA-2B1010739).

Compliance with ethical standards

Conflict of interest The authors declare that they have no conflict of interest.

Publisher's note Springer Nature remains neutral with regard to jurisdictional claims in published maps and institutional affiliations.

References

1. Yamaguchi M, Suzuki R, Oguchi M. Advances in the treatment of extranodal NK/T-cell lymphoma, nasal type. *Blood*. 2018; 131:2528–40.
2. Wolchok JD, Chiarion-Sileni V, Gonzalez R, Rutkowski P, Grob JJ, Cowey CL, et al. Overall survival with combined nivolumab and ipilimumab in advanced melanoma. *N Engl J Med*. 2017;377:1345–56.
3. Zappasodi R, Merghoub T, Wolchok JD. Emerging concepts for immune checkpoint blockade-based combination therapies. *Cancer Cell*. 2018;33:581–98.
4. Pardoll DM. The blockade of immune checkpoints in cancer immunotherapy. *Nat Rev Cancer*. 2012;12:252–64.
5. Mellman I, Coukos G, Dranoff G. Cancer immunotherapy comes of age. *Nature*. 2011;480:480–9.
6. Garon EB, Rizvi NA, Hui R, Leigh N, Balmanoukian AS, Eder JP, et al. Pembrolizumab for the treatment of non-small-cell lung cancer. *N Engl J Med*. 2015;372:2018–28.
7. Swerdlow SH, Campo E, Harris NL, Jaffe ES, Pileri SA, Stein H, et al. WHO classification of tumours of haematopoietic and lymphoid tissues. 4th ed. Lyon: IARC; 2017.
8. Wang H, Wang L, Liu WJ, Xia ZJ, Huang HQ, Jiang WQ, et al. High post-treatment serum levels of soluble programmed cell death ligand 1 predict early relapse and poor prognosis in extranodal NK/T cell lymphoma patients. *Oncotarget*. 2016;7:33035–45.
9. Lai J, Xu P, Jiang X, Zhou S, Liu A. Successful treatment with anti-programmed-death-1 antibody in a relapsed natural killer/T-cell lymphoma patient with multi-line resistance: a case report. *BMC Cancer*. 2017;17:507.
10. Li X, Cheng Y, Zhang M, Yan J, Li L, Fu X, et al. Activity of pembrolizumab in relapsed/refractory NK/T-cell lymphoma. *J Hematol Oncol*. 2018;11:15.
11. Kim SJ, Hyeon J, Cho I, Ko YH, Kim WS. Comparison of Efficacy of Pembrolizumab between Epstein-barr Viruspositive and Negative Relapsed Or Refractory Non-hodgkin Lymphomas. *Cancer Res Treat*. 2018;51:611–22.
12. Kwong YL, Chan TSY, Tan D, Kim SJ, Poon LM, Mow B, et al. PD1 blockade with pembrolizumab is highly effective in relapsed or refractory NK/T-cell lymphoma failing l-asparaginase. *Blood*. 2017;129:2437–42.
13. Song TL, Nairismagi ML, Laurensia Y, Lim JQ, Tan J, Li ZM, et al. Oncogenic activation of the STAT3 pathway drives PD-L1 expression in natural killer/T-cell lymphoma. *Blood*. 2018;132:1146–58.
14. Jo JC, Kim M, Choi Y, Kim HJ, Kim JE, Chae SW, et al. Expression of programmed cell death 1 and programmed cell death ligand 1 in extranodal NK/T-cell lymphoma, nasal type. *Ann Hematol*. 2017;96:25–31.
15. Nagato T, Ohkuri T, Ohara K, Hirata Y, Kishibe K, Komabayashi Y, et al. Programmed death-ligand 1 and its soluble form are highly expressed in nasal natural killer/T-cell lymphoma: a potential rationale for immunotherapy. *Cancer Immunol Immunother*. 2017;66:877–90.
16. Kim WY, Jung HY, Nam SJ, Kim TM, Heo DS, Kim CW, et al. Expression of programmed cell death ligand 1 (PD-L1) in advanced stage EBV-associated extranodal NK/T cell lymphoma is associated with better prognosis. *Virchows Arch*. 2016;469:581–90.
17. Chen BJ, Chapuy B, Ouyang J, Sun HH, Roemer MG, Xu ML, et al. PD-L1 expression is characteristic of a subset of aggressive B-cell lymphomas and virus-associated malignancies. *Clin Cancer Res*. 2013;19:3462–73.
18. Roach C, Zhang N, Corigliano E, Jansson M, Toland G, Ponto G, et al. Development of a companion diagnostic PD-L1 immunohistochemistry assay for pembrolizumab therapy in non-small-cell lung cancer. *Appl Immunohistochem Mol Morphol*. 2016;24:392–7.
19. Daud AI, Wolchok JD, Robert C, Hwu WJ, Weber JS, Ribas A, et al. Programmed death-ligand 1 expression and response to the anti-programmed death 1 antibody pembrolizumab in melanoma. *J Clin Oncol*. 2016;34:4102–9.
20. Muro K, Chung HC, Shankaran V, Geva R, Catenacci D, Gupta S, et al. Pembrolizumab for patients with PD-L1-positive advanced gastric cancer (KEYNOTE-012): a multicentre, open-label, phase 1b trial. *Lancet Oncol*. 2016;17:717–26.
21. Kim SJ, Yoon DH, Jaccard A, Chng WJ, Lim ST, Hong H, et al. A prognostic index for natural killer cell lymphoma after non-anthracycline-based treatment: a multicentre, retrospective analysis. *Lancet Oncol*. 2016;17:389–400.
22. Waggott D, Chu K, Yin S, Wouters BG, Liu FF, Boutros PC. NanoStringNorm: an extensible R package for the pre-processing of NanoString mRNA and miRNA data. *Bioinformatics*. 2012; 28:1546–8.
23. Robinson MD, McCarthy DJ, Smyth GK. edgeR: a bioconductor package for differential expression analysis of digital gene expression data. *Bioinformatics*. 2010;26:139–40.
24. Zhang NN, Chen JN, Xiao L, Tang F, Zhang ZG, Zhang YW, et al. Accumulation mechanisms of CD4(+)CD25(+)FOXP3(+) regulatory T cells in EBV-associated gastric carcinoma. *Sci Rep*. 2015;5:18057.
25. Wingate PJ, McAulay KA, Anthony IC, Crawford DH. Regulatory T cell activity in primary and persistent Epstein-Barr virus infection. *J Med Virol*. 2009;81:870–7.
26. Morales O, Mrizak D, Francois V, Mustapha R, Miroux C, Depil S, et al. Epstein-Barr virus infection induces an increase of T regulatory type 1 cells in hodgkin lymphoma patients. *Br J Haematol*. 2014;166:875–90.
27. Li S, Gowans EJ, Chougnat C, Plebanski M, Dittmer U. Natural regulatory T cells and persistent viral infection. *J Virol*. 2008;82:21–30.
28. Gobert M, Treilleux I, Bendriss-Vermare N, Bachelot T, Goddard-Leon S, Arfi V, et al. Regulatory T cells recruited through CCL22/CCR4 are selectively activated in lymphoid infiltrates surrounding

- primary breast tumors and lead to an adverse clinical outcome. *Cancer Res.* 2009;69:2000–9.
29. Kim WY, Jeon YK, Kim TM, Kim JE, Kim YA, Lee SH, et al. Increased quantity of tumor-infiltrating FOXP3-positive regulatory T cells is an independent predictor for improved clinical outcome in extranodal NK/T-cell lymphoma. *Ann Oncol.* 2009;20:1688–96.
 30. Ritprajak P, Azuma M. Intrinsic and extrinsic control of expression of the immunoregulatory molecule PD-L1 in epithelial cells and squamous cell carcinoma. *Oral Oncol.* 2015;51:221–8.
 31. Abiko K, Matsumura N, Hamanishi J, Horikawa N, Murakami R, Yamaguchi K, et al. IFN-gamma from lymphocytes induces PD-L1 expression and promotes progression of ovarian cancer. *Br J Cancer.* 2015;112:1501–9.
 32. Mimura K, Teh JL, Okayama H, Shiraishi K, Kua LF, Koh V, et al. PD-L1 expression is mainly regulated by interferon gamma associated with JAK-STAT pathway in gastric cancer. *Cancer Sci.* 2018;109:43–53.
 33. Qu QX, Huang Q, Shen Y, Zhu YB, Zhang XG. The increase of circulating PD-L1-expressing CD68(+) macrophage in ovarian cancer. *Tumour Biol.* 2016;37:5031–7.
 34. Wherry EJ. T cell exhaustion. *Nat Immunol.* 2011;12:492–9.
 35. Schreiber RD, Old LJ, Smyth MJ. Cancer immunoeediting: integrating immunity's roles in cancer suppression and promotion. *Science.* 2011;331:1565–70.
 36. O'Donnell JS, Teng MWL, Smyth MJ. Cancer immunoeediting and resistance to T cell-based immunotherapy. *Nat Rev Clin Oncol.* 2018;16:151–67.
 37. Aragon-Sanabria V, Kim GB, Dong C. From cancer immunoeediting to new strategies in cancer immunotherapy: the roles of immune cells and mechanics in oncology. *Adv Exp Med Biol.* 2018;1092:113–38.
 38. Nobre CC, de Araujo JM, Fernandes TA, Cobucci RN, Lanza DC, Andrade VS, et al. Macrophage migration inhibitory factor (MIF): biological activities and relation with cancer. *Pathol Oncol Res.* 2017;23:235–44.
 39. Simpson KD, Templeton DJ, Cross JV. Macrophage migration inhibitory factor promotes tumor growth and metastasis by inducing myeloid-derived suppressor cells in the tumor microenvironment. *J Immunol.* 2012;189:5533–40.
 40. Yaddanapudi K, Rendon BE, Lamont G, Kim EJ, Al Rayyan N, Richie J, et al. MIF is necessary for late-stage melanoma patient MDSC immune suppression and differentiation. *Cancer Immunol Res.* 2016;4:101–12.
 41. Yaddanapudi K, Putty K, Rendon BE, Lamont GJ, Faughn JD, Satoskar A, et al. Control of tumor-associated macrophage alternative activation by macrophage migration inhibitory factor. *J Immunol.* 2013;190:2984–93.